ACS APPLIED MATERIALS & INTERFACES

Research Article

www.acsami.org

Nanostructured Materials Prepared by Surface-Assisted Reduction: New Catalysts for Methane Oxidation

A. Gomathi,[†] Susan M. Vickers,[†] Rahman Gholami,[§] Mina Alyani,[§] Renee W. Y. Man,[†] Mark J. MacLachlan,*[,†] Kevin J. Smith,*[,§] and Michael O. Wolf*[,†]

[†]Department of Chemistry, University of British Columbia, 2036 Main Mall, Vancouver, British Columbia V6T 1Z1, Canada

[§]Department of Chemical and Biological Engineering, University of British Columbia, 2360 East Mall, Vancouver, British Columbia V6T 1Z3, Canada

Supporting Information

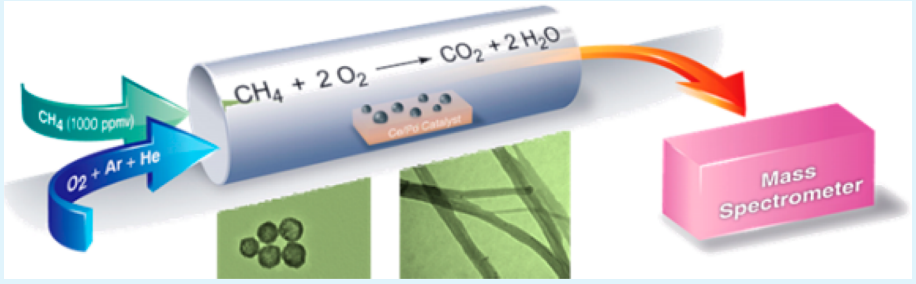

ABSTRACT: Cerium formate hollow spheres and cerium hydroxycarbonate nanorods with residual formate groups are effective for reducing palladium(II) salts onto their surfaces. Calcination of the new materials obtained by this surface-assisted reduction method gives highly active PdO/CeO_2 nanostructures with Pd well dispersed on the substrate. Temperature-programmed oxidation experiments showed that these nanomaterials are good catalysts for the low-temperature oxidation of methane, with 50% conversion temperatures ($T_{50\%}$) at ~300 °C.

KEYWORDS: *nanostructured materials, surface-assisted reduction, methane oxidation, cerium oxide, palladium*

INTRODUCTION

Natural gas is an abundant, clean-energy alternative to gasoline and diesel as it produces less CO_2 per unit energy.[1] However, the management of unburned methane from natural gas engines is a growing concern because methane is a potent greenhouse gas with a global warming potential ~25 times greater than CO_2.[2] As conventional catalytic convertors are unable to efficiently remove methane at the low exhaust temperature of natural gas-powered vehicles, there is a great demand for new materials to function as low-temperature methane oxidation catalysts. New materials that catalyze methane oxidation at low temperature (<300 °C) will be required to meet future emission standards for natural gas vehicles and to treat industrial emissions.[3] This is currently an active area of research with many new materials being explored.[4−8]

Noble metal catalysts have the potential for reduced NO_x emissions and complete methane oxidation at low temperatures, combined with the ease of integration into existing vehicles.[9,10] Unfortunately, three-way catalytic convertors currently used in vehicles are poor at oxidizing methane. Among the most promising materials for this process are Pd/CeO_2 composites.[11−13] Ceria is an ideal support for methane oxidation catalysis as an accessible Ce^{3+}/Ce^{4+} redox cycle gives it high oxygen storage capacity (OSC) and high oxygen mobility, both of which can stabilize Pd or Pt on ceria and enhance catalytic oxidation. Electron and oxygen transfer studies on model Pt/CeO_2 catalysts show favorable interactions on nanostructured ceria that enhance activity,[14] and the hydrophobicity of ceria may help stabilize it under the harsh conditions found in exhaust streams.[15] Pd/CeO_2 materials are typically formed by wet impregnation methods, but other methods including coprecipitation, deposition−precipitation, specific adsorption, and combustion synthesis have also been explored.[12,16−19] These methods, however, generally lead to ill-defined structures and relatively high initiation temperatures (light-off temperatures) for catalytic methane oxidation. Improvements such as assembly of $Pd@CeO_2$ core−shell particles on alumina have resulted in catalysts with improved performance,[20] but developing catalysts that are active below ~300 °C remains a daunting challenge.

We have discovered a straightforward method for constructing highly active PdO/CeO_2 nanostructured materials with outstanding catalytic activities. This new family of catalysts is prepared by a 2-step procedure, where a ceria precursor (either cerium hydroxycarbonate, CHC, or cerium formate, CF) is first

Received: June 12, 2015
Accepted: August 11, 2015
Published: August 19, 2015

DOI: 10.1021/acsami.5b05189
ACS Appl. Mater. Interfaces 2015, 7, 19268−19273

formed (Figure 1) then reacted with a palladium salt. Fortuitous incorporation of formate groups allows the surface-assisted reduction (SAR) of Pd^{2+} on the ceria precursor surface without the need for an added reducing agent, giving nanostructured PdO/CeO_2 composites after thermolysis. This method leads to excellent dispersion of the PdO on the substrate. Temperature-programmed oxidation (TPO) measurements show that these new materials have excellent performance in the catalytic oxidation of methane, with light-off temperatures ($T_{50\%}$) of <300 °C and complete combustion around 400 °C. These highly active nanostructured catalytic materials prepared by our new approach could be important for helping reduce global natural gas emissions.

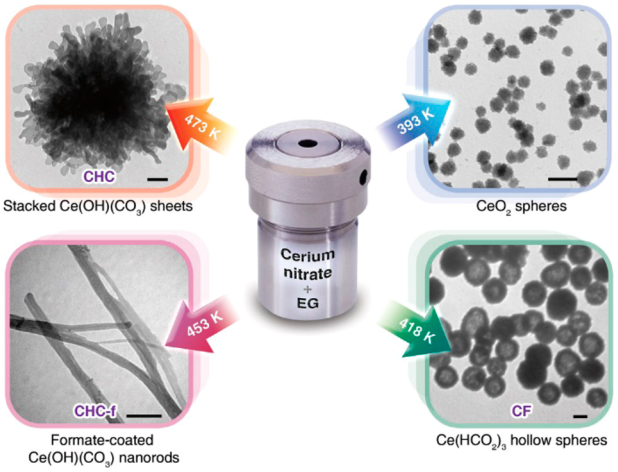

Figure 1. Synthesis of new nanostructured cerium-containing materials. At low temperature, cerium nitrate in EG gives ceria spheres. As the temperature is increased during preparation, decomposition products of EG, including formic acid and carbon dioxide, yield CF hollow spheres, formate-coated CHC nanorods (CHC-f), and CHC with a stacked-sheet morphology. The scale bar in the TEM images corresponds to 100 nm.

RESULTS AND DISCUSSION

Nanostructured forms of CHC ($Ce(OH)CO_3$) and CF ($Ce(HCOO)_3$) were prepared by solvothermal reaction between cerium nitrate and ethylene glycol (EG). EG is known to be a reducing agent that can be oxidized to aldehydes, acids, and, finally, CO_2.[21,22] By varying only the reaction temperature, different cerium-containing products that incorporate these intermediates were obtained. The synthesis of the different nanostructured ceria precursors is illustrated in Figure 1, and electron microscopy images of the hollow spheres and nanorods are shown in Figure 2.

Cerium nitrate and EG reacted at temperatures below 393 K and produced crystalline ceria nanospheres. When the reaction was carried out at 418 K, CF nanospheres were obtained, confirmed by powder X-ray diffraction (PXRD; Figure 2A–C). The FT-IR spectrum (Figure S2) of the product showed an intense band at 1570 cm^{-1} that is characteristic of the asymmetric COO stretching mode and a band at 776 cm^{-1} that arises from δ (OCO) of the formate group, along with the bands due to residual EG (~1040–1080 cm^{-1}).[23,24] This temperature was clearly sufficient for the oxidation of EG to formic acid, which led to the formation of cerium formate.

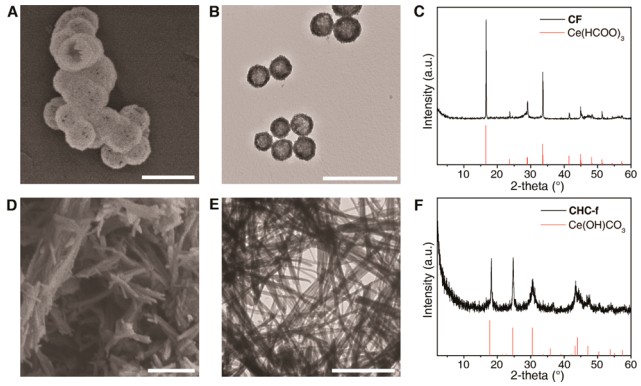

Figure 2. Electron microscopy images and PXRD patterns of as-synthesized cerium-based nanostructures obtained from the reaction of cerium nitrate with EG. (A) Field-emission scanning electron microscopy (FESEM) image of as-synthesized (418 K) hollow spheres of CF. (B) Transmission electron microscopy (TEM) image of CF, showing the hollow spheres. (C) PXRD pattern of CF. The PXRD pattern matches that of cerium formate, JCPDS 49-1245 (red). (D) FESEM image of CHC-f nanofibers synthesized at 453 K. (E) TEM image of CHC-f. (F) PXRD pattern of CHC-f, which matches JCPDS-52-0352 (red). The scale bars in the electron micrographs correspond to 500 nm.

Reactions carried out at 453 K resulted in a yellow gel consisting of CHC nanorods as confirmed by PXRD (Figure 2D–F). X-ray photoelectron spectroscopy (XPS; Table S1 and Figures S6–7) of this material showed only the presence of cerium in oxidation state +3, as expected for CHC. XPS of the CHC nanorods showed an O 1s peak characteristic of hydroxycarbonates.[25] Notably, FT-IR spectroscopy (Figure S2) of the CHC nanorods revealed the presence of formate along with bands due to the hydroxycarbonate and residual EG. Formic acid and carbon dioxide are known decomposition products of EG, and the formate coats the CHC product (the CHC nanorods coated with formate are denoted as CHC-f). CHC was also formed at 473 K, but this material had a sheet-like morphology and was more crystalline than the nanorods (Figure S1). Also, IR spectroscopy (Figure S2) showed that CHC had comparably less residual formate and EG than the CHC-f nanorods.

Upon calcination at 673 K, all of the precursors gave ceria nanostructures with retention of morphology. Calcining CF hollow spheres resulted in hollow ceria nanospheres (ceria-ns), while CHC-f gave ceria nanorods (ceria-nr). PXRD analysis indicated the products are microcrystalline and XPS data were consistent with CeO_2, demonstrating that this is a facile route to nanostructured forms of ceria with different morphologies.

While our work was in progress,[26] He et al. described the preparation of hollow spheres of a mixture of CHC/CF from heating cerium nitrate in EG, but they did not observe the CF fibers that we obtained.[27] These results validate our finding that the phase behavior of cerium nitrate in EG is complex and can give rise to diverse nanostructured materials.

With new nanostructured forms of CHC and CF in hand, we set out to combine these with Pd in order to generate active catalyst materials. Figure 3A shows the general scheme for the SAR reaction and photographs of the starting material and product. To our surprise, the addition of either CHC-f or CF hollow spheres to aqueous solutions of palladium nitrate yielded black precipitates, indicating a reduction of Pd^{2+} to Pd^0. Sodium formate has been reported as an efficient reducing

DOI: 10.1021/acsami.5b05189
ACS Appl. Mater. Interfaces 2015, 7, 19268–19273

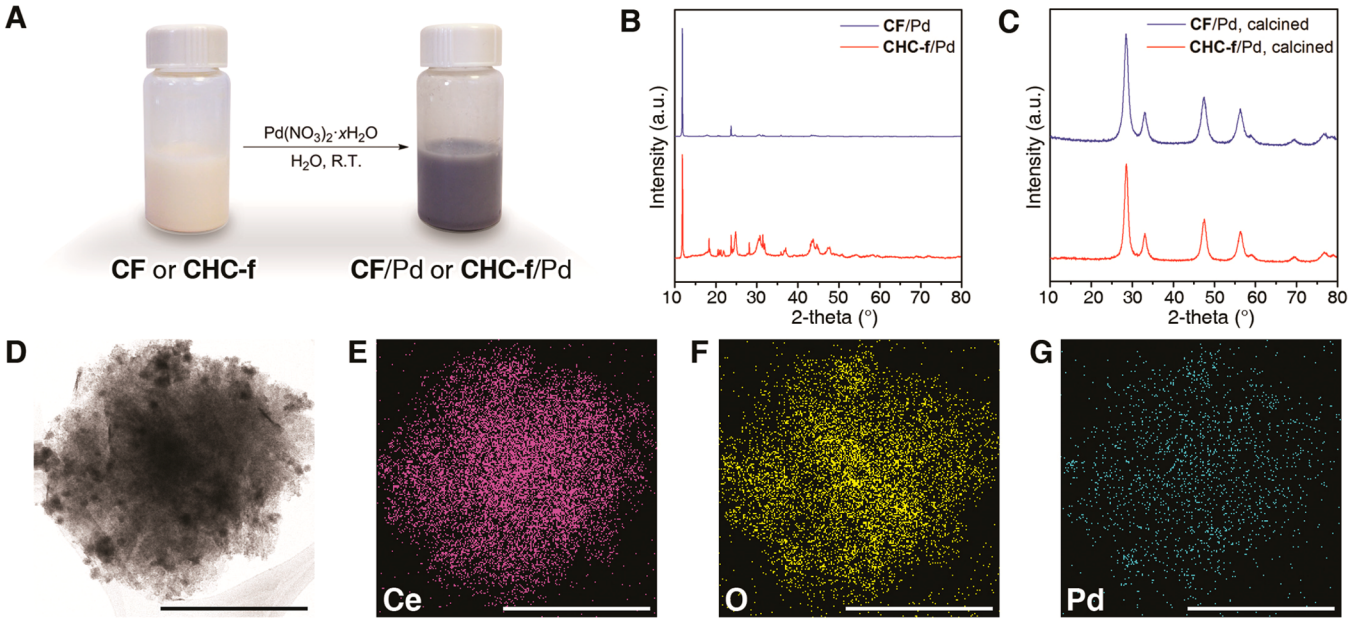

Figure 3. Synthesis and characterization of the Pd/ceria nanostructures. (A) The reaction of CF or CHC-f with 1 mM of Pd^{2+} gives black precipitates of as-synthesized CF/Pd(1 mM) or CHC-f/Pd(1 mM). (B) PXRD of the two samples, as synthesized CF/Pd(1 mM) and CHC-f/Pd(1 mM). (C) PXRD of the two samples, CF/Pd(1 mM) and CHC-f/Pd(1 mM), after calcination at 673 K. (D) Scanning transmission electron microscope (STEM) image of CHC-f/Pd(1 mM) obtained after calcination at 673 K and the corresponding energy dispersive X-ray spectroscopy (EDS) elemental maps of (E) Ce, (F) O, and (G) Pd. The scale bars in the electron micrographs correspond to 500 nm.

agent in the synthesis of palladium nanoparticles,[28,29] and the formate appears to be responsible for the reduction of Pd^{2+} here. Qualitatively, the rate of the SAR correlated well with the relative proportion of formate groups present in the CHC-f or CF. When CF was used as the precursor, the SAR was rapid, and the solution turned black in less than 5 min. On the other hand, when the CHC synthesized at 453 K (CHC-f) was used as precursor, the solution turned black only after 60 min. When CHC prepared at a high temperature (with no detectable formate on its surface) was used, the SAR took ~12 h. With pure ceria and CHC prepared by a urea route there was no visible reduction of the Pd^{2+}, even after 2 days. Reduction of palladium nitrate is facilitated by formate groups on CHC-f or CF, depositing palladium on the surface of the nanostructured ceria precursors.

FT-IR spectra of CF and the product obtained after reaction with palladium nitrate (Figure S3) shows that after reduction, the characteristic peaks of formate (1570 and 776 cm^{-1}) disappear and new peaks characteristic of carbonate (1385 and 847 cm^{-1}) appear. Thus, reduction of the Pd^{2+} by formate yields carbonate as a byproduct.

The PXRD patterns (Figure 3B) of the solids obtained using CHC-f or CF as precursor are both dominated by low angle reflections at 2θ = 11.7, 23.4, and 35°, and do not show reflections due to crystalline palladium or palladium oxide. The PXRD patterns do not have sufficient peaks to index to a unit cell, but they have characteristic patterns that are similar to layered metal oxide structures.[30,31] In the case of CHC-f, after the reaction with palladium nitrate, the PXRD pattern of the sample showed reflections of both CHC and the lamellar structure. Interestingly, CHC-f stirred in water for 12 h without added palladium nitrate also transformed into the same crystalline structure (Figure S4). When the CF or CHC sample prepared at 473 K was treated with water, there was no indication of the layered structure forming.

On the basis of these results, we believe that the carbonate and residual EG facilitate the transformation of the precursors into layered materials in water. When the as-synthesized cerium formate is stirred with water, it has the residual EG needed to form the layered structure but lacks the carbonate. On the other hand, CHC synthesized at 473 K has sufficient carbonate but no residual EG, and therefore does not form the layered structure; this is corroborated by the FT-IR data in Figure S2. Thus, the formation of the layered structure occurs only when both the carbonate and some residual EG are present in the reaction mixture. For comparison, we prepared cerium formate by reacting cerium chloride with formic acid in ethanol. Cerium formate prepared by this EG-free route also reduced palladium nitrate. The PXRD pattern of the sample (Figure S12) obtained after reduction did not have peaks due to palladium or its compounds. There is also no indication of the formation of the layered structure. The postreduction sample was a mixture of cerium formate and cerium carbonate, which supports the conclusion that the formate takes part in the reduction, yielding carbonate as the byproduct. Because there was no EG present in the reaction, the product was cerium carbonate, not the layered structure.

High-resolution XPS spectra of the Ce 3d region of CHC-f after water treatment and after SAR with $Pd(NO_3)_2$ are both similar to the XPS spectrum of as-synthesized CF, confirming that neither the water treatment nor the reaction with palladium nitrate results in the oxidation of Ce^{3+} to Ce^{4+}. This shows that the reduction of palladium involves the formate groups and the Ce^{3+} does not act as reducing agent. High-resolution XPS data (Figure S10) of the product show the presence of Pd^0.[32,33]

The sample obtained after in situ reduction of 1 mM palladium nitrate on CHC-f was calcined at 673 K to prepare a 1 wt % Pd-CeO_2 catalyst (denoted as CHC-f/Pd(1 mM)). The PXRD pattern of the calcined sample was indexed to cubic

DOI: 10.1021/acsami.5b05189
ACS Appl. Mater. Interfaces 2015, 7, 19268−19273

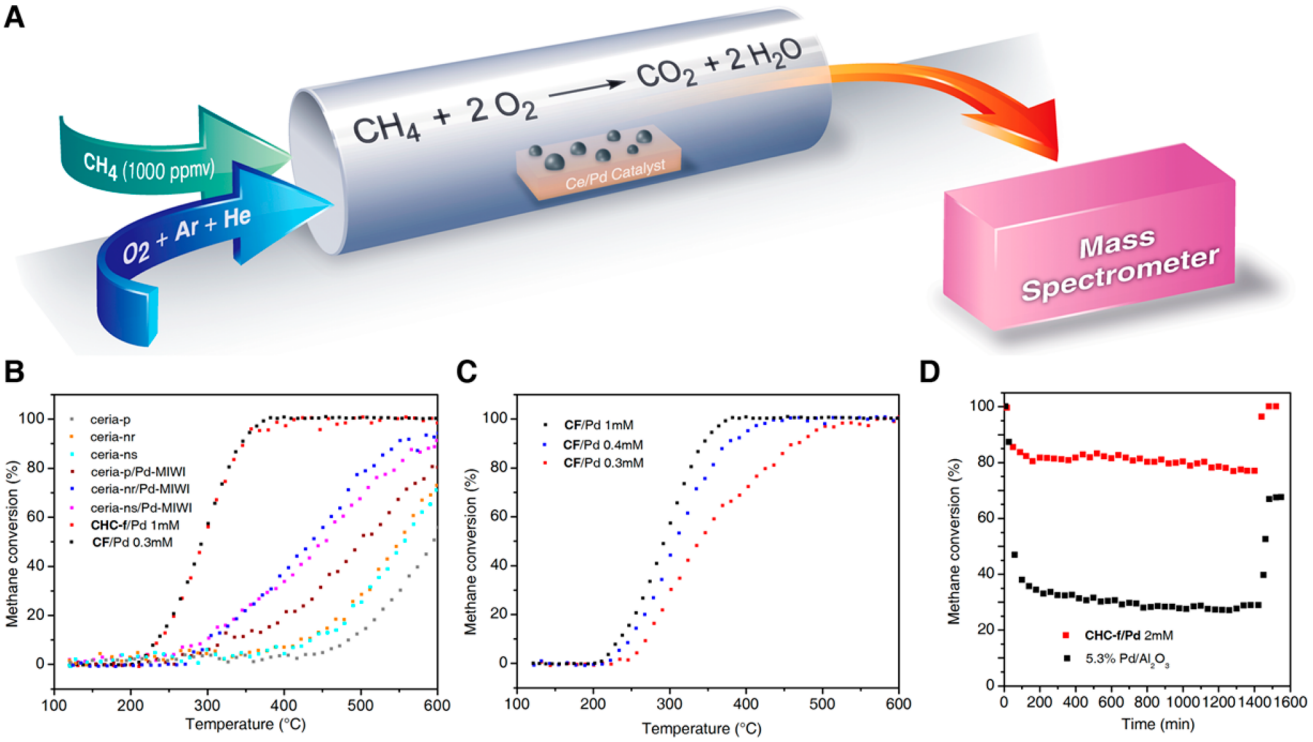

Figure 4. TPO reaction of ceria and ceria/Pd materials. (A) Schematic of the TPO reaction, where methane is oxidized over a bed of the catalyst to give carbon dioxide and water. (B) TPO of methane in the presence of different catalyst samples (nr = nanorods; ns = nanospheres; p = precipitated; ceria-x/Pd-MIWI = ceria in form x with 1% Pd deposited by the MIWI method; CHC-f/Pd(1 mM), CF/Pd(0.3 mM) = samples prepared with 1% Pd by in situ reduction, as described in the text). Reaction conditions: 1000 ppmv CH_4 in 20% O_2 (balance He and Ar); space velocity, 180 000 mL(STP)·g^{-1}·h^{-1}. (C) TPO of methane in the presence of CeO_2/Pd samples with different reduction rates of Pd^{2+} by CF (sample prepared by in situ reduction of Pd^{2+} by varying concentrations of $Pd(NO_3)_2$; CF/Pd(1 mM) = 1 mM; CF/Pd(0.4 mM) = 0.4 mM; CF/Pd(0.3 mM) = 0.3 mM). The palladium loading of the final composite was adjusted to be 1 wt %. Reaction conditions: 1000 ppmv CH_4 in 20% O_2 (balance He and Ar); Space velocity 180 000 mL(STP)·g^{-1}·h^{-1}. (D) Steady-state oxidation of methane in the presence of water (5% water), using CHC-f/Pd or 5.3 wt % Pd/Al_2O_3 as the catalyst. Water was introduced at t = 0 min and switched off after 24 h. Reaction conditions: 5000 ppmv CH_4 in 20% O_2 (balance He and Ar); space velocity, 180 000 mL (STP)·g^{-1}·h^{-1} at T = 380 °C.

CeO_2, and no peaks for Pd or PdO were observed (Figure 3C). The EDX spectrum (Figure S5) of the calcined sample shows the presence of both Ce and Pd. TEM images of the CHC-f/Pd(1 mM) sample show that after calcination, the material has lost the nanofibrillar morphology of the CHC-f precursor (Figure 2E) and appears as sheets (Figure 3D). XPS data of CHC-f/Pd(1 mM) shows predominantly Ce^{4+}, as expected, and the O 1s XPS data are similar to ceria. The high-resolution Pd 3d XPS spectrum of CHC-f/Pd(1 mM) calcined at 673 K shows that most of the palladium is present as PdO (B.E. = 337 eV). A small contribution from a second peak with a higher B.E. = 338.1 eV is also present. The higher B.E. value indicates a more ionic form of palladium; this has been reported to arise due to the interaction of palladium with the ceria matrix.[32] In the CeO_2/Pd samples prepared by the formate-assisted method, the palladium mainly exists as palladium oxide, and some palladium exhibits ionic character from the interaction with the ceria.

The catalytic activities of the ceria nanostructures and nano ceria-supported palladium catalysts were measured by passing methane and oxygen over a bed of the material and monitoring the products formed by mass spectrometry (Figure 4A). These conditions were chosen to mimic the exhaust gas composition from a natural gas vehicle in terms of O_2 content and CH_4 concentration. To assess the effect of nanostructuring of the ceria, bulk ceria was prepared by the traditional precipitation method (ceria-p). For comparison of palladium loading methods, 1% Pd-loaded reference samples were prepared by the modified incipient wet impregnation (MIWI) technique. Samples prepared from various ceria nanostructures and palladium nitrate by MIWI are denoted as ceria-x/Pd-MIWI (x = nr for nanorods, ns for nanospheres, and p for precipitation) after calcination. The CeO_2/Pd samples prepared by in situ formate reduction of palladium nitrate with cerium precursors followed by calcination are denoted as indicated in Table S2. The mass spectroscopic analysis confirmed the presence of both H_2O and CO_2 in the reactor products, but neither CO nor H_2 were detected for any of the catalyst samples reported herein. This confirms that the water gas shift reaction did not occur to any extent under the conditions used here.

The temperature profiles for methane conversion using CHC-f/Pd(1 mM), CF/Pd(0.3 mM) and control catalyst samples prepared by MIWI are shown in Figure 4B. CHC-f/Pd(1 mM) and CF/Pd(0.3 mM) show excellent activity with a $T_{50\%}$ (temperature at which 50% conversion occurs) for the samples well below 300 °C and $T_{100\%}$ (temperature at which conversion is complete) of 400 °C. By comparison, the other ceria-x/Pd-MIWI samples examined have $T_{50\%}$ > 400 °C and complete conversion was not achieved even at 600 °C. Significantly, the CHC-f/Pd(1 mM) and CF/Pd(0.3 mM) samples exhibit substantially better activity than the samples prepared by the MIWI method. A comparison of the materials prepared by SAR to other Pd/CeO_2 catalysts in fixed-bed

DOI: 10.1021/acsami.5b05189
ACS Appl. Mater. Interfaces 2015, 7, 19268−19273

Table 1. Comparison of Catalyst Performance

catalyst	T_{50} (°C)	Pd (wt %)	catalyst mass (mg)	total flow (mL(STP)/min)	GHSV (mL/(g h))[a]	ref
CHC-f/Pd(1 mM)	< 300	1	100	300	180 000	present work
Pd@CeO_2	320	1	50	83	199 200	20
PdO on mesoporous aluminosilica	377−453	0.6−2.0	100	100	120 000	35

[a]GHSV (gas hourly space velocity) = total volumetric flow rate (mL/h)/catalyst mass(g) = mL/(g·h).

reactor studies (Table 1) shows that our catalyst shows comparable results to these systems.

We believe that one important reason for the outstanding catalytic activity in these materials is the dispersion of the formate groups on the surface of the ceria-precursor nanostructures, which leads to good dispersion of the Pd nanoparticles and enhances metal−support interactions. Although we could not observe nanoparticles by TEM or by PXRD, we carried out STEM-EDS mapping (Figure 3E−G) to show that the palladium oxide is well-dispersed in the ceria matrix. To further prove that dispersion is important, we prepared samples with different concentrations of palladium nitrate. When the SAR was performed on CHC-f using 2 mM $Pd(NO_3)_2$ (CHC-f/Pd(2 mM)), the solution turned black in 15 min (as opposed to 60 min if 1 mM $Pd(NO_3)_2$ was used). When CF is used as the cerium precursor in 1 mM $Pd(NO_3)_2$ solution, reduction occurs in less than 5 min (CF/Pd(1 mM)), whereas the CF in 0.4 and 0.3 mM $Pd(NO_3)_2$ reduces Pd^{2+} in 15 and 30 min, respectively. The samples are named based on the $Pd(NO_3)_2$ concentration as (CF/Pd(0.4 mM) and CF/Pd(0.3 mM)). In each case, the final product contained 1 wt % Pd.

The catalytic efficiency of CeO_2/Pd samples prepared by varying the palladium nitrate concentration in the surface-assisted reduction of Pd^{2+} by CF is shown in Figure 4C. When CF is used as precursor, the catalytic activity of the samples increases as the palladium source is diluted: CF/Pd(0.3 mM) > CF/Pd(0.4 mM) > CF/Pd(1 mM). The reaction with diluted palladium nitrate solution results in slower reduction and thereby slower nucleation of Pd^0. Because no external capping agents are used, slower reduction leads to less aggregation and better dispersion of Pd^0. The dispersion of the Pd formed upon reduction apparently depends on the reduction conditions and cerium precursor, resulting in differing activities. In general, the slower the reduction, the better the catalytic activity of the composite. Slower reduction may increase the number of catalytic sites accessible to the methane and improve the redox interaction between the Pd and ceria.

Pd-substrate interactions have been demonstrated to be important for methane oxidation reactions as the substrate provides oxygen for the reaction and can mediate deactivation pathways.[33] Recent work has indicated that the hydrophobicity of CeO_2 may be important for enhancing its stability even in the presence of water.[15] Figure 4D shows the methane conversion efficiency of CHC-f/Pd(2 mM) containing 1 wt % Pd (prepared by SAR) versus an Al_2O_3/Pd catalyst containing 5.3 wt % Pd and prepared by the conventional MIWI method. Upon the introduction of water, both catalysts show decreased performance, as previously reported,[34] but the decrease for the CHC-f/Pd catalyst is only ~20%, compared to a ~ 70% reduction for the Al_2O_3/Pd catalyst. After 24 h, the hydrothermal treatment was ended and subsequently the CHC-f/Pd catalyst fully recovered its activity, whereas the Al_2O_3/Pd catalyst only partially recovered after the test. These initial results demonstrate that the CHC-f/Pd catalysts are highly active and show very good hydrothermal stability.

CONCLUSIONS

We report a new family of ceria nanostructures with interesting and controllable morphologies that are readily prepared by combining cerium-containing precursors in ethylene glycol with nitric acid. We have also found a new way to synthesize palladium-based catalytic nanomaterials by surface-assisted reduction (SAR), taking advantage of the reduction potential of formate groups incorporated on ceria nanostructures. This is the first report of the surface-assisted reduction of palladium salts by a cerium precursor for the synthesis of Pd/CeO_2 catalysts. This discovery has led to new nanostructured catalyst precursors with controlled deposition of palladium on their surfaces, without the need for an additional reducing agent. After calcination, the Pd/CeO_2 catalysts show impressive catalytic performance for methane oxidation, with ignition temperatures ($T_{50\%}$) of <300 °C. The enhanced performance of these materials when compared to materials made by other techniques likely arises from the good dispersion of Pd nanoparticles on the catalyst surface. Considering the importance of PdO-based materials in industrial catalysis, these new materials may be useful for applications in catalytic converters, natural gas furnaces, and industrial methane scrubbing.

ASSOCIATED CONTENT

Supporting Information

The Supporting Information is available free of charge on the ACS Publications website at DOI: 10.1021/acsami.5b05189.

Detailed synthesis procedures, characterization details, TPO conditions, tabulated XPS data, supplementary PXRD, IR, EDX, and XPS spectra. (PDF)

AUTHOR INFORMATION

Corresponding Authors

*E-mail: mmaclach@chem.ubc.ca.
*E-mail: kjs@mail.ubc.ca.
*E-mail: mwolf@chem.ubc.ca.

Author Contributions

M.J.M. and M.O.W. supervised the materials development and K.J.S. supervised the catalyst testing. A.G. and S.M.V. carried out the synthesis of cerium compound nanostructures. A.G. synthesized palladium−ceria catalysts. R.G. and K.J.S. carried out catalyst testing and data interpretation. A.G. and R.W.Y.M. carried out characterization of the materials. M.A. carried out the hydrothermal stability test of the materials. A.G., M.J.M., and M.O.W. wrote the manuscript. All the authors discussed and commented on the manuscript.

Notes

The authors declare no competing financial interest.

DOI: 10.1021/acsami.5b05189
ACS Appl. Mater. Interfaces 2015, 7, 19268−19273

■ ACKNOWLEDGMENTS

We thank the Natural Sciences and Engineering Research Council (NSERC) of Canada, the Government of British Columbia for a Natural Resources and Applied Sciences (NRAS) grant, and Westport Power, Inc., for funding. We are grateful to Sandeep Munshi and Alan Welch (Westport) for useful discussions.

■ REFERENCES

(1) DeLuchi, M. A. *Emissions of Greenhouse Gases from the use of Ttransportation Fuels and Electricity*. Center for Transportation Research, Argonne National Laboratory, Argonne, IL, 1991.
(2) Howarth, R.; Santoro, R.; Ingraffea, A. Methane and the Greenhouse-gas Footprint of Natural Gas from Shale Formations. *Clim. Change* **2011**, *106*, 679−690.
(3) Gélin, P.; Primet, M. Complete Oxidation of Methane at Low Temperature over Noble Metal based Catalysts: A Review. *Appl. Catal., B* **2002**, *39*, 1−37.
(4) Fujimoto, K.; Ribeiro, F. H.; Avalos-Borja, M.; Iglesia, E. Structure and Reactivity of PdO_x/ZrO_2 Catalysts for Methane Oxidation at Low Temperatures. *J. Catal.* **1998**, *179*, 431−442.
(5) Jiminez-Borja, C.; Delgado, B.; Dorado, F.; Valverde, J. L. Experimental data and Kinetic modeling of the Catalytic and Electrochemically Promoted CH_4 Oxidation over Pd Catalyst-electrodes. *Chem. Eng. J.* **2013**, *225*, 315−322.
(6) Wasalathanthri, N. D.; Poyraz, A. S.; Biswas, S.; Meng, Y.; Kuo, C.-H.; Kriz, D. A.; Suib, S. L. High-performance Catalytic CH_4 Oxidation at Low Temperatures: Inverse Micelle Synthesis of Amorphous Mesoporous Manganese Oxides and Mild Transformation to $K_{2-x}Mn_8O_{16}$ and ε-MnO_2. *J. Phys. Chem. C* **2015**, *119*, 1473−1482.
(7) Gholami, R.; Smith, K. J. Activity of PdO/SiO_2 Catalysts for CH_4 Oxidation following Thermal Treatments. *Appl. Catal., B* **2015**, *169-169*, 156−163.
(8) Fiuk, M. M.; Adamski, A. Activity of MnO_x−CeO_2 Catalysts in Combustion of Low Concentrated Methane. *Catal. Today* **2015**, *39*, in press. DOI: 10.1016/j.cattod.2015.01.029.
(9) Anderson, R. B.; Stein, K. C.; Feenan, J. J.; Hofer, L. J. E. Catalytic Oxidation of Methane. *Ind. Eng. Chem.* **1961**, *53*, 809−812.
(10) Sekizawa, K.; Widjaja, H.; Maeda, S.; Ozawa, Y.; Eguchi, K. Low Temperature Oxidation of Methane over Pd Catalyst Supported on Metal Oxides. *Catal. Today* **2000**, *59*, 69−74.
(11) Bozo, C.; Guilhaume, N.; Herrmann, J.-M. Role of the Ceria−Zirconia Support in the Reactivity of Platinum and Palladium Catalysts for Methane Total Oxidation under Lean Conditions. *J. Catal.* **2001**, *203*, 393−406.
(12) Colussi, S.; Gayen, A.; Farnesi Camellone, M.; Boaro, M.; Llorca, J.; Fabris, S.; Trovarelli, A. Nanofaceted Pd−O Sites in Pd−Ce Surface Superstructures: Enhanced Aactivity in Catalytic Combustion of Methane. *Angew. Chem., Int. Ed.* **2009**, *48*, 8481−8484.
(13) Mayernick, A. D.; Janik, M. J. Methane Oxidation on Pd−Ceria: A DFT Study of the Mechanism over $Pd_xCe_{1-x}O_2$, Pd, and PdO. *J. Catal.* **2011**, *278*, 16−25.
(14) Vayssilov, G. N.; Lykhach, Y.; Migani, A.; Staudt, T.; Petrova, G. P.; Tsud, N.; Skála, T.; Bruix, A.; Illas, F.; Prince, K. C.; Matolín, V. r.; Neyman, K. M.; Libuda, J. Support Nanostructure Boosts Oxygen Transfer to Catalytically Active Platinum Nanoparticles. *Nat. Mater.* **2011**, *10*, 310−315.
(15) Azimi, G.; Dhiman, R.; Kwon, H.-M.; Paxson, A. T.; Varanasi, K. K. Hydrophobicity of Rare-Earth Oxide Ceramics. *Nat. Mater.* **2013**, *12*, 315−320.
(16) Le Normand, F.; Hilaire, L.; Kili, K.; Krill, G.; Maire, G. Oxidation State of Cerium in Cerium-based Catalysts Investigated by Spectroscopic Probes. *J. Phys. Chem.* **1988**, *92*, 2561−2568.
(17) Luo, M.-F.; Hou, Z.-Y.; Yuan, X.-X.; Zheng, X.-M. Characterization Study of CeO_2 Supported Pd Catalyst for Low-Temperature Carbon monoxide Oxidation. *Catal. Lett.* **1998**, *50*, 205−209.
(18) Shen, W.-J.; Ichihashi, Y.; Matsumura, Y. A Comparative Study of Palladium and Copper Catalysts in Methanol Synthesis. *Catal. Lett.* **2002**, *79*, 125−127.
(19) Thevenin, P. O.; Alcalde, A.; Pettersson, L. J.; Järås, S. G.; Fierro, J. L. G. Catalytic Combustion of Methane over Cerium-doped Palladium Catalysts. *J. Catal.* **2003**, *215*, 78−86.
(20) Cargnello, M.; Jaén, J. J. D.; Garrido, J. C. H.; Bakhmutsky, K.; Montini, T.; Gámez, J. J. C.; Gorte, R. J.; Fornasiero, P. Exceptional Activity for Methane Combustion over Modular $Pd@CeO_2$ Subunits on Functionalized Al_2O_3. *Science* **2012**, *337*, 713−717.
(21) Bock, C.; Paquet, C.; Couillard, M.; Botton, G. A.; MacDougall, B. R. Size-selected Synthesis of PtRu Nano-catalysts: Reaction and Size Control Mechanism. *J. Am. Chem. Soc.* **2004**, *126*, 8028−8037.
(22) Jiang, X.; Wang, Y.; Herricks, T.; Xia, Y. Ethylene Glycol-Mediated Synthesis of Metal Oxide Nanowires. *J. Mater. Chem.* **2004**, *14*, 695−703.
(23) Ferraro, J. R.; Becker, M. I.R. Investigation of Several Rare-earth Acetates and Formates. *J. Inorg. Nucl. Chem.* **1970**, *32*, 1495−1500.
(24) Harvey, K. B.; Morrow, B. A.; Shurvell, H. F. The Infrared Absorption of some Crystalline Inorganic formates. *Can. J. Chem.* **1963**, *41*, 1181−1187.
(25) Yang, J.; Cheng, H.; Frost, R. L. Synthesis and Characterisation of Cobalt Hydroxy Carbonate $Co_2CO_3(OH)_2$ Nanomaterials. *Spectrochim. Acta, Part A* **2011**, *78*, 420−428.
(26) MacLachlan, M. J.; Wolf, M. O.; Anandhanatarajan, G. Methods of Preparing Metal/Metal Oxide Materials from Nanostructured Substrates and Uses Thereof. U.S. Provisional Pat. Appl. 61/944,876, 2014. PCT Appl. filed Feb 2015.
(27) He, L.; Li, J.; Feng, Z.; Sun, D.; Wang, T.; Li, R.; Xu, Y. Solvothermal Synthesis and Characterization of Ceria with Solid and Hollow Spherical and Multilayered Morphologies. *Appl. Surf. Sci.* **2014**, *322*, 147−154.
(28) Wang, Z.-L.; Yan, J.-M.; Wang, H.-L.; Ping, Y.; Jiang, Q. Pd/C synthesized with citric acid: An Efficient Catalyst for Hydrogen Generation from Formic Acid/Sodium Formate. *Sci. Rep.* **2012**, *2*, 598.
(29) Zhong, L.-S.; Hu, J.-S.; Cui, Z.-M.; Wan, L.-J.; Song, W.-G. In-situ Loading of Noble Metal Nanoparticles on Hydroxyl-group-rich Titania Precursor and their Catalytic Applications. *Chem. Mater.* **2007**, *19*, 4557−4562.
(30) Larcher, D.; Sudant, G.; Patrice, R.; Tarascon, J. M. Some Insights on the use of Polyols-based Metal Alkoxides Powders as Precursors for Tailored Metal-Oxides Particles. *Chem. Mater.* **2003**, *15*, 3543−3551.
(31) Zhong, L.-S.; Hu, J.-S.; Cao, A.-M.; Liu, Q.; Song, W.-G.; Wan, L.-J. 3D Flowerlike Ceria Micro/Nanocomposite Structure and its Application for Water Treatment and CO Removal. *Chem. Mater.* **2007**, *19*, 1648−1655.
(32) Priolkar, K. R.; Bera, P.; Sarode, P. R.; Hegde, M. S.; Emura, S.; Kumashiro, R.; Lalla, N. P. Formation of $Ce_{1-x}Pd_xO_{2-\delta}$ Solid Solution in Combustion-Synthesized Pd/CeO_2 Catalyst: XRD, XPS, and EXAFS Investigation. *Chem. Mater.* **2002**, *14*, 2120−2128.
(33) Schwartz, W. R.; Pfefferle, L. D. Combustion of Methane over Palladium-based Catalysts: Support Interactions. *J. Phys. Chem. C* **2012**, *116*, 8571−8578.
(34) Persson, K.; Pfefferle, L. D.; Schwartz, W.; Ersson, A.; Järås, S. G. Stability of Palladium-Based Catalysts during Catalytic Combustion of Methane: The Influence of Water. *Appl. Catal., B* **2007**, *74*, 242−250.
(35) Gannouni, A.; Albela, B.; Zina, M. S.; Bonneviot, L. Metal Dispersion, Accessibility and Catalytic Activity in Methane Oxidation of Mesoporous Templated Aluminosilica Supported Palladium. *Appl. Catal., A* **2013**, *464−465*, 116−127.

DOI: 10.1021/acsami.5b05189
ACS Appl. Mater. Interfaces 2015, 7, 19268−19273